The International Journal of Advanced Manufacturing Technology (2019) 103:1911–1923
https://doi.org/10.1007/s00170-019-03660-y

ORIGINAL ARTICLE

Smooth flank milling tool path generation for blade surfaces considering geometric constraints

Yao-An Lu[1] · Cheng-Yong Wang[1] · Li Zhou[2] · Jian-Bo Sui[1] · Li-Juan Zheng[1]

Received: 5 October 2018 / Accepted: 27 March 2019 / Published online: 13 April 2019

Abstract
In practical machining, flank milling path generation methods of blade surfaces should concern machine axes' motions to improve machined surface quality, as well as the gouging-avoidance with the hub surface and the geometric deviation constraints. The smoothness of the tool orientation in the part coordinate system cannot assure the smooth rotary axis motions of a five-axis machine tool, since the conversion of tool orientation from the part coordinate system to the machine coordinate system is nonlinear. A flank milling path is represented with the cutter reference point trajectory and the displacement curves of the two rotary axes in this research, so that the machine axes' motions along the tool path can be directly smoothed when generating the path. The point-to-surface distance function is adopted to evaluate the geometric deviation, and an algorithm based on the differential evolution algorithm is presented to solve the distance function robustly. The sum of the squares of the first, second, and third derivatives of the cutter reference point trajectory and the two rotary axes' displacement curves are adopted as the smoothness indicators. Then, a flank milling path generation model for blade surface smoothing the machine axes' motions and considering the hub surface gouging-avoidance and geometric deviations constraints is developed. Numerical examples and machining experiments for five-axis flank milling of a blade surface are given to confirm the validity and effectiveness of the proposed approach.

Keywords Flank milling · Smooth tool path · Geometric deviations · Rotary axes · Geometric constraints

1 Introduction

Fans, compressors, and impellers are the main components of turbo-machinery. At present, blade surfaces of these turbo-machinery parts are mainly manufactured by five-axis computer numerical control (CNC) milling with two distinct methods: point milling and flank milling. Flank milling comparatively outweighs point milling in several respects: higher material removal rate, elimination of hand finish, and so on. Therefore, five-axis flank milling has been widely applied in blade surface machining.

Many researchers have studied the methods of impeller machining. Fan et al. [1] presented five-axis flank milling tool path generation methods in rough and semi-finish machining for centrifugal impeller with arbitrary blade surfaces. Focused on blade finishing, Calleja et al. [2] described a cutting force prediction method of blade flank milling. Later, they developed a flank milling path generation method for freeform surfaces with ball-end cutters, and the method can compute patches that well approximate the input freeform surface [3]. Tapered ball-end cutters are usually employed in impeller machining because of its high stiffness. Moreover, the blade surface and the fillet can be machined in a single pass using the ball-end cutters, and the ball-end of the cutters should be tangent to the hub surface to avoid gouging. Lu et al. [4] developed a model to optimize the geometry of conical cutters for impeller flank milling. Based on the on-machine measurement inspection system, Huang et al. [5] introduced an integrated machining deviation compensation strategy, which can be used in the blade surface machining.

High surface finish quality and accuracy are the fundamental requirements for blade surface flank milling. Dramatic changes in machine axes' motions from one cutter location to another one will result in poor surface quality by leaving

✉ Yao-An Lu
luyaoan@gdut.edu.cn

[1] School of Electromechanical Engineering, Guangdong University of Technology, Guangzhou 510006, China

[2] School of Electromechanical Engineering, Guangdong Polytechnic Normal University, Guangzhou 510635, China

tool marks. The surface quality could be improved by minimizing the accelerations and the vibrations of the machine tool components. Due to the complexity of the inverse kinematical transformation (IKT) of five-axis machine tools, it is difficult to anticipate the machine tool kinematical behavior during tool path generation [6]. Therefore, researchers prefer to smooth the tool path, mainly the tool orientation, in the part coordinate system (PCS) [7–10]. However, considering the structure of five-axis machine tools and the kinematical characteristics of the joints, smooth tool orientations in the PCS do not necessarily mean smooth motions of the rotary axes of the machine tool. It is especially the case at the singular point of the five-axis machine tool. At the singular point, slight changes of the tool orientation in the PCS may cause a great rotation of the machine axes, no matter how smooth the tool orientations in the PCS are [6, 11]. Therefore, the issue of smoothing the machine axes' motions should be concerned.

In five-axis machining, different methods were proposed to smooth the rotary axes' motions. Based on the domain of admissible orientation (DAO) concept, Castagnetti et al. [12] optimized the rotary axis movements for tool path generation. Taking the physical limits of the drives into account, Beudaert et al. [13] proposed an algorithm to iteratively smooth the joint motions along the tool path to raise the real feed rate. Plakhotnik et al. [14] developed an optimization method of finding a sequence of tool orientations that can minimize the displacements of the machine rotary axes. Lin et al. [15] described a method of avoiding singularities by translating the tool orientations in the configuration-space (C-space), and the orientation polyline was translated by a minimum translating vector to avoid the singularities. Later, they developed a modified particle swarm optimization algorithm to find an optimal translating vector in the C-space to control the machined surface textures as well as the machining errors [16]. Geng et al. [17] generated smooth tool paths for sculptured surface machining by considering the joint movements between two neighboring cutter locations in the machine tool frame. Hu et al. [18] presented a new five-axis tool path generation algorithm taking the specific machine tool's kinematic and dynamic loading constraints into consideration. Srijuntongsiri et al. [19] revealed a method to minimize the kinematic error in five-axis machining by inserting additional cutter locations between key cutter locations and rotating/translating the part surface into an optimal position. Lu et al. [20] developed a smooth flank milling path generation method based on the gradient-based differential evolution method, considering the rotary axis motions of the five-axis machine tool. The control points of the tool axis trajectory surface represented in the PCS were optimized to smooth the two rotary axis movements. Later, they also presented a smoothing approach, which was applied directly to the rotary axis motions [21]. However, the constraint of gouging-avoidance with the hub surface for blade surface milling path generation is not concerned in these two methods. Besides, the trajectory of the cutter reference point was not optimized neither. Finding the collision-free tool orientations in the C-space, Mi et al. [22] then introduced a difference graph to find a smoother tool orientation.

The tool path generation algorithm should not only take the performance of the machine tool into account but also respect the geometric deviations of the tool path. It is especially true for five-axis flank milling tool path of blade surfaces. Lartigue et al. [23] developed a flank milling tool path deformation method to make the envelope surface fit the ideal surface as much as possible, and only the geometric deviations were concerned. The methods proposed in Refs. [7, 10] increased the tool path smoothness by minimizing the strain energy of the tool axis trajectory surface. However, the tool path smoothing was realized in the PCS, and the machine axes' movements were not taken into account. Affouard et al. [11] proposed an algorithm to deform the tool path avoiding the tool transitioning in the singular cone, and the displacements applied to the control points were limited, so that the actual tool path still satisfied the given geometric tolerance. However, this algorithm was applied to point milling, not flank milling.

The deformation method is usually employed to optimize and correct the flank milling tool path, mainly reducing the geometric deviations between the envelope surface and the design surface. The geometric deviations and the smooth movements of the machine axes should be confronted simultaneously when deforming a tool path. Besides, different from planning a flank milling path for a single surface, the hub surface gouging-avoidance constraint should be concerned as well for blade surfaces milling path generation. The cutter's ball-end should be tangent to the hub surface at the corresponding cutter contact point, thereby ensuring it does not gouge the hub surface. Different from the previous research, a flank milling tool path in this research is represented with the cutter reference point trajectory in the PCS and the displacement curves of the two rotary axes of the used machine tool. Then, the smoothing optimization in this research is applied directly in the rotary axis movements, and the cutter reference point trajectory is also optimized. Moreover, the geometric deviations and the hub surface gouging-avoidance constraints are also taken into account.

The remainder of this paper is organized as follows. The preliminaries for five-axis flank milling path generation are presented in Sect. 2, including the tool path representation method and the point-to-surface distance function based tool path optimization method. In Sect. 3, the smoothness tool path indicators and the geometric constraints are introduced, and

the model and algorithm for smoothness tool path optimization are described as well. Numerical examples and machining experiments are presented in Sect. 4, and conclusions are given in Sect. 5.

2 Preliminaries

2.1 Tool path representation

The geometric model of a tapered ball-end cutter is shown in Fig. 1a, and the ball center c is selected as the cutter reference point. The parameters of the cutter are ball radius of the tool r_{ball}, tapered angle φ, and cutter length H. The cutter surface can be constructed by using a one-parameter family of spheres, as shown in Fig. 1b. The radius r of any sphere can be expressed as

$$r(a) = r_{\text{ball}} + a{\cdot}\sin\varphi \tag{1}$$

where a is the distance between the associated sphere center and the cutter reference point c, and $a \in [a_0, a_1] = \left[0, \left((H - r_{\text{ball}}){\cdot}\tan(\varphi) + \frac{r_{\text{ball}}}{\cos(\varphi)}\right){\cdot}\tan(\varphi) + (H - r_{\text{ball}})\right]$.

Each cutter location along a tool path consists of a position and a unit orientation. The position constitutes the cutter reference point trajectory when the cutter moves along the tool path. When the cutter location data of the tool path is obtained, the IKT of the particular five-axis machine tool is used to convert the cutter location data into NC code, acquiring the rotary axes' positions. Therefore, a five-axis milling path can be represented by three B-spline curves, which are the spline $\boldsymbol{P}(u)$ for the cutter reference point trajectory in the PCS and the other two splines represent the movements of the two rotary axes along the tool path. The tool orientation curve $\boldsymbol{O}(u)$ of a path can be represented with the two rotary axis displacements, as shown in Fig. 2b. For an AC-type table-tilting machine tool, $\boldsymbol{O}(u)$ can be expressed as

$$\boldsymbol{O}(u) = \begin{bmatrix} O_{\text{i}}(u) \\ O_{\text{j}}(u) \\ O_{\text{k}}(u) \end{bmatrix} = \begin{bmatrix} \sin(C_{\text{C}}(u)){\cdot}\sin(C_{\text{A}}(u)) \\ \cos(C_{\text{C}}(u)){\cdot}\sin(C_{\text{A}}(u)) \\ \cos(C_{\text{A}}(u)) \end{bmatrix} \tag{2}$$

where $C_{\text{A}}(u)$, $C_{\text{C}}(u)$ are the displacement curves of the two rotary axes of the specified machine tool along the tool path, which can be calculated by interpolating the rotary axes' positions of the discrete cutter location data along the tool path. To synchronize the tool reference point position and tool orientation, the knot vector of $\boldsymbol{P}(u)$ and $\boldsymbol{O}(u)$ are identical. Therefore, the tool axis trajectory surface of a flank milling tool path can be expressed as Eq. (3),

$$\boldsymbol{S}_{\text{axis}}(\boldsymbol{w}; v, u) = \boldsymbol{P}(u) + v{\cdot}\boldsymbol{O}(u) \tag{3}$$

where $\boldsymbol{w} = [w_0, \ldots, w_{\text{m}-1}]^T \in \mathbb{R}^{\text{m}}$ denotes the control points of $\boldsymbol{P}(u)$ and $\boldsymbol{O}(u)$ and $v \in [0, H - r_{\text{ball}}]$ for ball-end cutters. Suppose the number of the control points of $\boldsymbol{P}(u)$ is l, then $m = 3l + l + l$.

The way to calculate the control points of $\boldsymbol{P}(u)$ and $\boldsymbol{O}(u)$ is described as follows. Let $\boldsymbol{c}_{\text{i}} (i = 0, 1, \ldots, l-1)$ denote the given cutter reference points along a path. The parameter values of $\boldsymbol{c}_{\text{i}} (i = 0, 1, \ldots, l-1)$ are calculated by using the chord-parameterization method, as the expression in Eq. (4).

$$\begin{cases} t_0 = 0, \\ t_k = t_{k-1} + \|\boldsymbol{c}_k - \boldsymbol{c}_{k-1}\|, k = 1, \ldots, l-1 \end{cases} \tag{4}$$

Then the knot vector $\{u_0, u_1, \ldots, u_{\text{n}}\} (n = l + p)$ can be evaluated with the parameter values $\{t_0, t_1, \ldots, t_{l-1}\}$ according to Eq. (5), where p denotes the degree of B-spline curve.

$$\begin{cases} u_0 = \cdots = u_{\text{p}} = 0, u_{\text{n-p}} = \cdots = u_{\text{n}} = t_{\text{l-1}}, \\ u_{\text{j}+p} = \dfrac{1}{p} \sum\limits_{\text{i}=j}^{\text{j+p-1}} t_i, j = 1, \ldots, l-1-p. \end{cases} \tag{5}$$

Then the control points can be obtained by solving linear equations, which can be referred to Ref. [24]. $[u_p, u_l]$ is the parameter domain of $\boldsymbol{P}(u)$ and $\boldsymbol{O}(u)$.

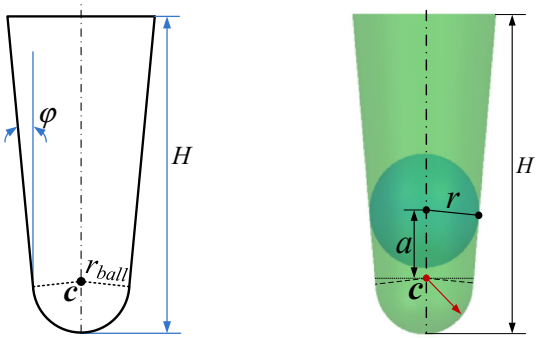

(a) Parameters of a tapered ball-end cutter (b) Cutter surface

Fig. 1 Geometric model of a tapered ball-end cutter

2.2 Representation of cutter swept envelope as a sphere-swept surface

A two-parameter family of spheres would be generated when the cutter moves along a tool path. The cutter swept surface is identically the envelope surface of this two-parameter family of spheres, as illustrated in Fig. 3. The radius r of any sphere in the family depends on the cutter shape, and $\boldsymbol{S}$ represents the trajectory surface of the sphere center. Both of them can be expressed as the following smooth functions of parameters a and u [25].

$$\boldsymbol{S}(\boldsymbol{w}; a, u) = \boldsymbol{S}_{\text{axis}}(\boldsymbol{w}; a, u), \quad r(\boldsymbol{w}; a, u) = r_{\text{ball}} + a{\cdot}\sin\varphi \tag{6}$$

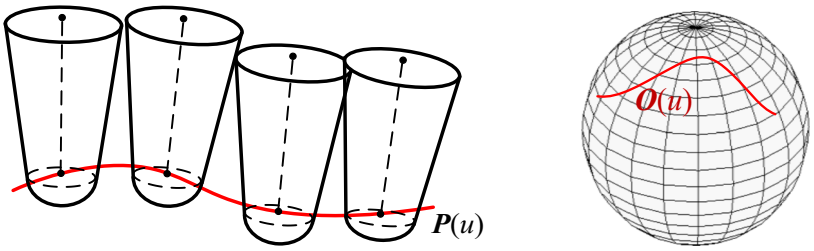

(a) Cutter reference point trajectory (b) Tool orientation curve

Fig. 2 Cutter reference point trajectory and tool orientation curve

where $u \in [u_p, u_l]$ and $a \in [a_0, a_1]$. More details can be found in Ref. [25].

2.3 Geometric deviation evaluation

For a flank milling tool path, the geometric deviation of a point on the design surface is defined as the signed orthogonal distance between the point to the cutter swept surface X, and the distance function can be calculated as

$$d_{\mathbf{p},X}(\boldsymbol{w}) = \text{sign} \cdot \min_{(a,u)} \|\boldsymbol{p} - \mathbf{X}(\boldsymbol{w}; a, u)\| \tag{7}$$

$d_{\mathbf{p},X}(\boldsymbol{w}) < 0$ and $d_{\mathbf{p},X}(\boldsymbol{w}) > 0$ indicate overcut and undercut, respectively. According to Refs. [25, 26], the geometric deviation of point $\boldsymbol{p}$ can be calculated as

$$d_{\mathbf{p},X}(\boldsymbol{w}) = \min_{(a,u)} \left(\|\boldsymbol{p} - \boldsymbol{S}(\boldsymbol{w}; a, u)\| - r(\boldsymbol{w}; a, u) \right) \tag{8}$$

The minimal value of Eq. (11) can be obtained by solving a system of nonlinear equations [25]. Since the tool path is represented with the two rotary axis displacement curves, it is complicated to find a good initial solution when solving the equations. Hence, an algorithm based on the different evolution (DE) algorithm is developed to solve Eq. (8), calculating the geometric deviation and the associated parametric coordinate (a, u) robustly. Details of the algorithm can be found in Appendix A, and more introductions of DE algorithm and its improved methods can be found in Refs. [27, 28]. The first-order differential increment of the distance function $d_{\mathbf{p},X}(\boldsymbol{w})$ with respect to the control points $\boldsymbol{w}$ can be computed as

$$\Delta d_{\mathbf{p},X}(\boldsymbol{w}) \approx \sum_{\mathrm{j}=0}^{\mathrm{m}-1} \left[\boldsymbol{S}_{w_j}(\boldsymbol{w}; a, u) \cdot \frac{\boldsymbol{S}(\boldsymbol{w}; a, u) - \boldsymbol{p}}{\|\boldsymbol{S}(\boldsymbol{w}; a, u) - \boldsymbol{p}\|} \right] \cdot \Delta w_{\mathrm{j}}$$
$$= -\left(\nabla d_{\mathbf{p},X}(\boldsymbol{w})\right)^{\mathrm{T}} \cdot (\Delta \boldsymbol{w}) \tag{9}$$

For more details on Eq. (9), the readers can refer to Ref. [25].

3 Model and algorithm for smoothness flank milling path generation

The smoothness of the tool path is a key criterion for blade surfaces flank milling. The object of tool positioning for blade surface flank milling is to seek a solution preserving smoothness of the tool path, while considering the geometric deviations and the hub surface gouging-avoidance constraints.

3.1 Smoothness indicators for the tool path

When a tool path is represented with Eq. (3), from the geometric point of view, the sum of the squares of the first,

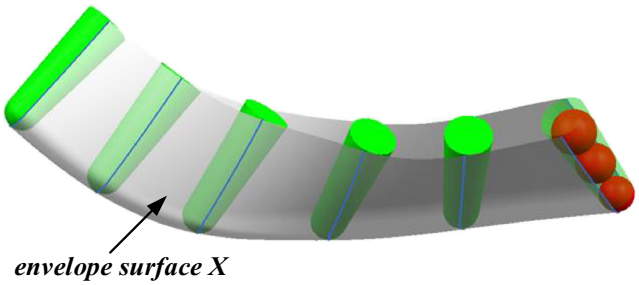

Fig. 3 Surface swept by a tapered ball-end cutter along a five-axis motion

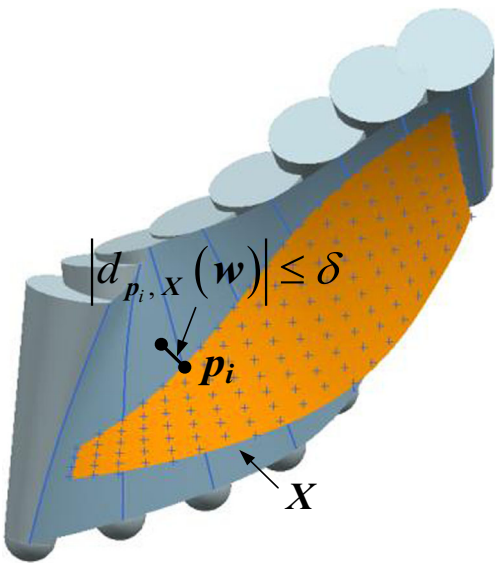

Fig. 4 Constraint of geometric deviations

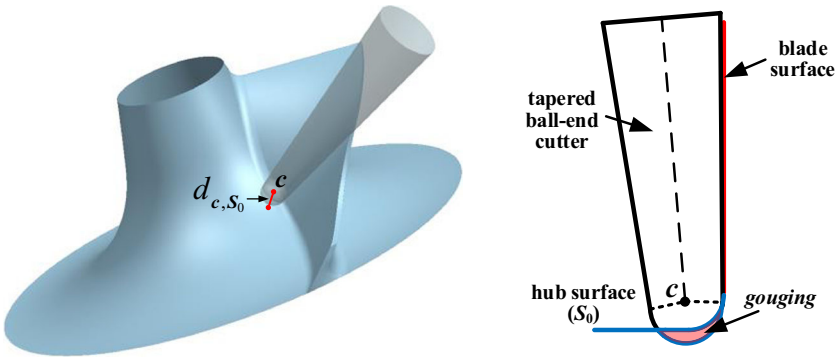

Fig. 5 Constraint of tangent the cutter's ball-end with the hub surface

second, and third derivatives of the three B-spline curves can be the indicators to denote the smoothness of the tool path, which are formulated in Eq. (10).

$$
\begin{aligned}
&F_{\text{first},A}=\int_{u_p}^{u_l}\left(\frac{dC_A(u)}{du}\right)^2du, \quad F_{\text{first},C}=\int_{u_p}^{u_l}\left(\frac{dC_C(u)}{du}\right)^2du, \quad F_{\text{second},A}=\int_{u_p}^{u_l}\left(\frac{d^2C_A(u)}{du^2}\right)^2du,\\
&F_{\text{second},C}=\int_{u_p}^{u_l}\left(\frac{d^2C_C(u)}{du^2}\right)^2du, \quad F_{\text{third},A}=\int_{u_p}^{u_l}\left(\frac{d^3C_A(u)}{du^3}\right)^2du, \quad F_{\text{third},C}=\int_{u_p}^{u_l}\left(\frac{d^3C_C(u)}{du^3}\right)^2du,\\
&F_{\text{first},pt}=\int_{u_p}^{u_l}\left(\frac{d\boldsymbol{P}(u)}{du}\right)^2du, \quad F_{\text{second},pt}=\int_{u_p}^{u_l}\left(\frac{d^2\boldsymbol{P}(u)}{du^2}\right)^2du, \quad F_{\text{third},pt}=\int_{u_p}^{u_l}\left(\frac{d^3\boldsymbol{P}(u)}{du^3}\right)^2du
\end{aligned}
\tag{10}
$$

The weighted sum method is the best known and simplest method for evaluating a number of alternatives in terms of a number of decision criteria. Therefore, it is used to score the smoothness of a given tool path, and its matrix form is expressed in Eq. (11),

$$F_{\text{smooth}}=\boldsymbol{D}_A{}^T\boldsymbol{K}_A\boldsymbol{D}_A+\boldsymbol{D}_C{}^T\boldsymbol{K}_C\boldsymbol{D}_C+\boldsymbol{D}_{pt}{}^T\boldsymbol{K}_{pt}\boldsymbol{D}_{pt} \tag{11}$$

where $B_{i,p}(u)$ is a B-spline basis function of degree p. $\boldsymbol{K}_A$, $\boldsymbol{K}_C$, $\boldsymbol{K}_{pt}$ are termed the stiffness matrices, and $\boldsymbol{K}_{A,ij}=\int_{u_p}^{u_l}(w_{\text{first}}\cdot B_{i,p}{}'(u)B_{j,p}{}'(u)+w_{\text{second}}\cdot B_{i,p}{}''(u)B_{j,p}{}''(u)+w_{\text{third}}\cdot B_{i,p}{}'''(u)\,B_{j,p}{}'''(u))du$, $0\le i,j\le l-1$. w_{first}, w_{second}, and w_{third} are the weights which are estimated to make $F_1=\boldsymbol{D}_A{}^T\boldsymbol{G}\boldsymbol{D}_A$, $F_2=\boldsymbol{D}_A{}^T\boldsymbol{L}\boldsymbol{D}_A$, and $F_3=\boldsymbol{D}_A{}^T\boldsymbol{R}\boldsymbol{D}_A$ have identical magnitude orders, where $\boldsymbol{G}_{ij}=\int_{u_p}^{u_l}(B_{i,p}{}'(u)B_{j,p}{}'(u))du$, $\boldsymbol{L}_{ij}=\int_{u_p}^{u_l}(B_{i,p}{}''(u)B_{j,p}{}''(u))du$, $\boldsymbol{R}_{ij}=\int_{u_p}^{u_l}(B_{i,p}{}'''(u)B_{j,p}{}'''(u))du$. In this work, $w_{\text{first}}=1/F_1$, $w_{\text{second}}=1/F_2$, $w_{\text{third}}=1/F_3$. $\boldsymbol{K}_C$ and $\boldsymbol{K}_{pt}$ can be estimated with the similar way. $\boldsymbol{D}_A\in\mathbb{R}^l$, $\boldsymbol{D}_C\in\mathbb{R}^l$, $\boldsymbol{D}_{pt}\in\mathbb{R}^{3l}$ are the control points of the two rotary axis displacement curves and the cutter reference point trajectory, respectively.

3.2 Constraint of geometric deviations

To satisfy the requirement of machining accuracy, the distance from a point on the design surface to the envelope surface swept by the cutter motions should be smaller than the tolerance δ. For a set of data points $\{\boldsymbol{p}_i\in\mathbb{R}^3, i=0,\cdots,n1\}$ sampled from the blade surface, we have the following constraint functions, as illustrated in Fig. 4.

$$C1 \quad |d_{\mathbf{p}_i,\boldsymbol{X}}(\boldsymbol{w})|\le\delta, \quad i=0,\cdots,n1 \tag{12}$$

3.3 Constraint of tangent the cutter's ball-end with the hub surface

When a ball-end cutter is used to mill blade surfaces, the ball-end of the cutter should be tangent to the hub surface at each cutter location, ensuring the cutter is gouge-free with the hub surface. As a result, the blade surface and the fillet are machined in a single pass. As illustrated in Fig. 5, $d_{\boldsymbol{c}_i,\boldsymbol{S}_0}(\boldsymbol{w})-r_{\text{ball}}=0$ means that the ball-end of the cutter is tangent to the hub surface $\boldsymbol{S}_0$. For a set of cutter reference points $\{\boldsymbol{c}_i\in\mathbb{R}^3, i=0,\cdots,n2\}$ sampled from $\boldsymbol{P}(u)$, we have the following constraint functions to avoid much material being left behind milling or the cutter gouging the hub surface,

$$C2 \quad |d_{\boldsymbol{c}_i,\boldsymbol{S}_0}(\boldsymbol{w})-r_{\text{ball}}|\le\varepsilon \quad i=0,\cdots,n2 \tag{13}$$

where ε is the prescribed tolerance.

3.4 Model for smoothness flank milling tool path optimization

The tool path can be applied a deformation, so that the envelope surface of the tool movement best fits the design surface

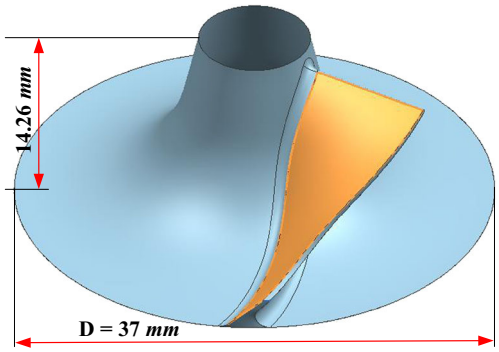

Fig. 6 The blade surface and the impeller model

[23]. Let $\{\boldsymbol{p}_i \in \mathbb{R}^3, 0 \le i \le n1\}$ and $\{\boldsymbol{c}_i \in \mathbb{R}^3, 0 \le i \le n2\}$ denote the point sets sampled from the design surface and $\boldsymbol{P}(u)$, respectively. The objective is to smooth the machine axes' motions while meeting the geometric constraints, including the geometric accuracy δ and the gouge-free between the cutter's ball-end and the hub surface. Therefore, it is a constrained nonlinear optimization problem (CNOP).

$$\begin{aligned} &\boldsymbol{P}1 \qquad\qquad s.t. \quad \min_{\mathrm{w}\in\mathbb{R}^{\mathrm{m}}} \quad F_{\mathrm{smooth}} \\ &|d_{\boldsymbol{p}_i,\boldsymbol{X}}(\boldsymbol{w})| \le \delta, \qquad i = 0, \cdots, n1 \\ &|d_{\boldsymbol{c}_i,\boldsymbol{S}_0}(\boldsymbol{w}) - r_{\mathrm{ball}}| \le \varepsilon, \quad i = 0, \cdots, n2 \end{aligned}$$

Sequential quadratic programming (SQP) is an iterative method for constrained nonlinear optimization and has been used successfully on many practical CNOP. The SQP method solves a sequence of optimization sub-problems, each of which optimizes a quadratic model of the objective subject to a linearization of the constraints. Here, we apply the SQP method to problem **P1**, and the sub-problem is the formula in **P2**.

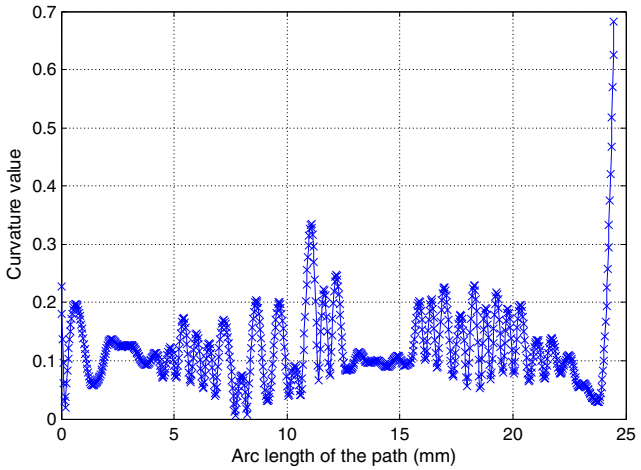

Fig. 8 The curvature plot for $\boldsymbol{P}(u)$ of the initial path

$$\begin{aligned} &\min_{\mathrm{w}\in\mathbb{R}^{\mathrm{m}}} \ (\Delta\boldsymbol{w})^{\mathrm{T}}\boldsymbol{Y}(\Delta\boldsymbol{w}) + (\Delta\boldsymbol{w})^{T}\boldsymbol{Y}\boldsymbol{w} \\ \boldsymbol{P}2 \quad s.t. \quad &-\delta \le d_{\mathbf{p}_i,\boldsymbol{X}}(\boldsymbol{w}) + \Delta d_{\boldsymbol{p}_i,\boldsymbol{X}}(\boldsymbol{w}) \le \delta, \qquad i = 0, \cdots, n1 \\ &-\varepsilon \le d_{\boldsymbol{c}_i,\boldsymbol{S}_0}(\boldsymbol{w}) - r_{\mathrm{ball}} + \Delta d_{\boldsymbol{c}_i,\boldsymbol{X}}(\boldsymbol{w}) \le \varepsilon, \quad i = 0, \cdots, n2 \end{aligned}$$

where

$$\boldsymbol{Y} = \begin{bmatrix} \boldsymbol{y}' & [\boldsymbol{0}]_{3l\times l} & [\boldsymbol{0}]_{3l\times l} \\ [\boldsymbol{0}]_{l\times l} & \lambda_{\mathrm{A}}\cdot\boldsymbol{K}_{\mathrm{A}} & [\boldsymbol{0}]_{l\times l} \\ [\boldsymbol{0}]_{l\times l} & [\boldsymbol{0}]_{l\times l} & \lambda_{\mathrm{C}}\cdot\boldsymbol{K}_{\mathrm{C}} \end{bmatrix}, \quad \boldsymbol{y}' = \begin{bmatrix} \lambda_{\mathrm{ls}}\cdot\boldsymbol{K}_{\mathrm{pt}} & [\boldsymbol{0}]_{l\times l} & [\boldsymbol{0}]_{l\times l} \\ [\boldsymbol{0}]_{l\times l} & \lambda_{\mathrm{ls}}\cdot\boldsymbol{K}_{\mathrm{pt}} & [\boldsymbol{0}]_{l\times l} \\ [\boldsymbol{0}]_{l\times l} & [\boldsymbol{0}]_{l\times l} & \lambda_{\mathrm{ls}}\cdot\boldsymbol{K}_{\mathrm{pt}} \end{bmatrix},$$

$\boldsymbol{w} = \begin{bmatrix} \boldsymbol{D}_{\mathrm{pt}} \\ \boldsymbol{D}_{\mathrm{A}} \\ \boldsymbol{D}_{\mathrm{C}} \end{bmatrix}$. The weightings λ_{ls}, λ_{A}, and λ_{C} are estimated to make the multiplied results $\lambda_{\mathrm{ls}}\cdot\boldsymbol{D}_{\mathrm{pt}}{}^{\mathrm{T}}\boldsymbol{K}_{\mathrm{pt}}\boldsymbol{D}_{\mathrm{pt}}$, $\lambda_{\mathrm{A}}\cdot\boldsymbol{D}_{\mathrm{A}}{}^{\mathrm{T}}\boldsymbol{K}_{\mathrm{A}}\boldsymbol{D}_{\mathrm{A}}$, and $\lambda_{\mathrm{C}}\cdot\boldsymbol{D}_{\mathrm{C}}{}^{\mathrm{T}}\boldsymbol{K}_{\mathrm{C}}\boldsymbol{D}_{\mathrm{C}}$ have the same magnitude orders. The weightings λ_{ls}, λ_{A}, and λ_{C} are change in each iteration. Moreover, the weights of determining the stiffness matrices $\boldsymbol{K}_{\mathrm{A}}$, $\boldsymbol{K}_{\mathrm{C}}$ and $\boldsymbol{K}_{\mathrm{pt}}$ are also change in each iteration. Now, we present the following algorithm for smoothness flank milling tool path generation.

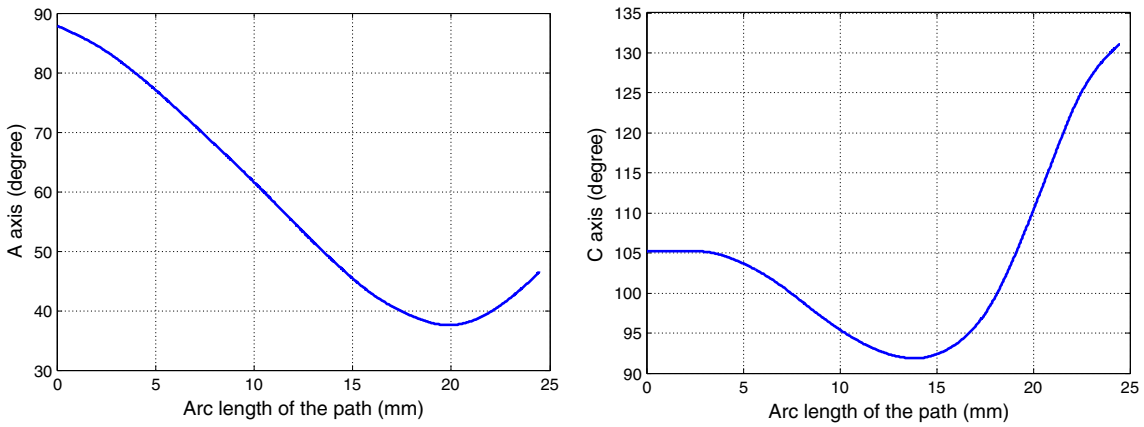

(a) Evolution of A axis (b) Evolution of C axis

Fig. 7 Evolutions of the two rotary axes along the initial path

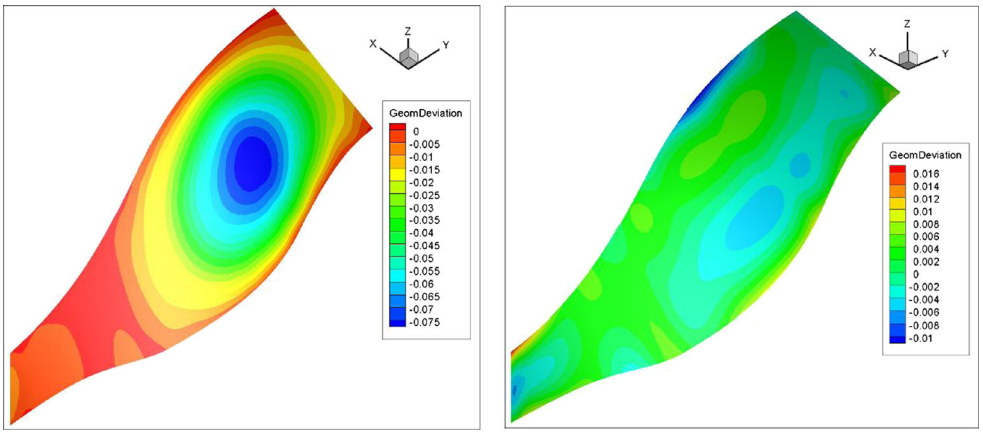

(a) (b)

Fig. 9 Distributions of the geometric deviations **a** before optimization and **b** after optimization

Algorithm

Input: The control points of the initial tool path $\boldsymbol{w}^0$; the knot vector and degree of B-spline curve; the prescribed tolerance δ and ε; the parameters of the tapered ball-end cutter; the maximal number of iterations T; the parameters used in the algorithm evaluating the geometric deviations.

Output: Optimum tool path $\boldsymbol{w}^*$.

Step 0:

(1) Set $k = 0$; (2) Compute the stiffness matrices $\boldsymbol{K}_A$, $\boldsymbol{K}_C$ and $\boldsymbol{K}_{pt}$ with the method described in Section 3.1; (3) Compute the smoothness indicators $\boldsymbol{D}_{pt}{}^T\boldsymbol{K}_{pt}\boldsymbol{D}_{pt}$, $\boldsymbol{D}_A{}^T\boldsymbol{K}_A\boldsymbol{D}_A$ and $\boldsymbol{D}_C{}^T\boldsymbol{K}_C\boldsymbol{D}_C$, and then determine the weightings λ_{ls}, λ_A and λ_C;

Step 1:

(1) Solve **P2** to determine the differential increment of the control points $\Delta\boldsymbol{w}$; (2) Update $\boldsymbol{w}^{k+1} = \boldsymbol{w}^k + \Delta\boldsymbol{w}$, and $\boldsymbol{D}_A, \boldsymbol{D}_C$ and $\boldsymbol{D}_{pt}$ are updated accordingly; (3) Update $\boldsymbol{K}_A$, $\boldsymbol{K}_C$, $\boldsymbol{K}_{pt}$, and then calculate $\boldsymbol{D}_{pt}{}^T\boldsymbol{K}_{pt}\boldsymbol{D}_{pt}$, $\boldsymbol{D}_A{}^T\boldsymbol{K}_A\boldsymbol{D}_A$ and $\boldsymbol{D}_C{}^T\boldsymbol{K}_C\boldsymbol{D}_C$, and then update λ_{ls}, λ_A and λ_C; (4) If $k <$ T, then set $k = k+1$ and go to 1(1); else exit and report $\boldsymbol{w}^* = \boldsymbol{w}^{k+1}$.

As with any nonlinear optimization problem, a good initial solution is needed when solving **P1**. Penalty methods are a certain class of algorithms for solving constrained optimization problems. They replace a constrained optimization problem by a series of unconstrained problems, and the unconstrained problems are formed by adding a term, called a penalty function. On the other hand, smoothing the rotary axes' motions of a machine tool needs to deform the tool path, and compromise has to be made between the smoothness and geometric deviations of the tool path. Hence, the weighted sum method is utilized, and the object function of tool path generation becomes

$$\mathbf{P3}\quad \min_{\mathrm{w}\in\mathbb{R}^{\mathrm{m}}} F = \lambda_{\mathrm{ls}}\cdot\sum_{\mathrm{i}=0}^{\mathrm{n1}}\left[d_{\mathbf{p}_i,X}(\boldsymbol{w})\right]^2 + \lambda_{\mathrm{A}}\cdot\boldsymbol{D}_{\mathrm{A}}{}^{\mathrm{T}}\boldsymbol{K}_{\mathrm{A}}\boldsymbol{D}_{\mathrm{A}} + \lambda_{\mathrm{C}}\cdot\boldsymbol{D}_{\mathrm{C}}{}^{\mathrm{T}}\boldsymbol{K}_{\mathrm{C}}\boldsymbol{D}_{\mathrm{C}} + \lambda_{\mathrm{pt}}\cdot\boldsymbol{D}_{\mathrm{pt}}{}^{\mathrm{T}}\boldsymbol{K}_{\mathrm{pt}}\boldsymbol{D}_{\mathrm{pt}} + \lambda_{\mathrm{penalty}}\cdot\sum_{\mathrm{i}=0}^{\mathrm{n2}}\left(d_{\boldsymbol{c}_i,\boldsymbol{s}_0}(\boldsymbol{w})-r_{\mathrm{ball}}\right)^2 \tag{14}$$

The Gauss-Newton method can be applied to solve Eq. (14), and the corresponding algorithm can be found in Appendix B.

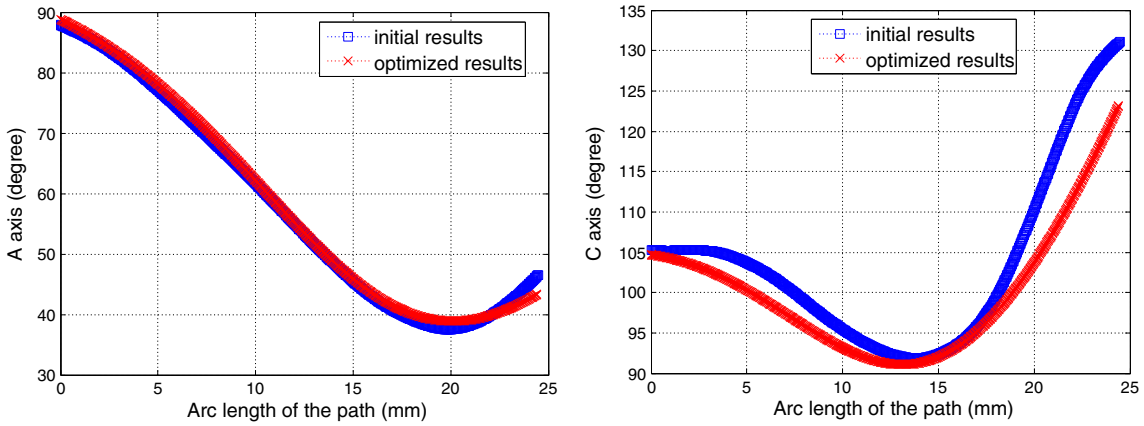

(a) Evolutions of A axis (b) Evolutions of C axis

Fig. 10 Evolutions of the two rotary axes along the optimized path

4 Simulations and machining experiments

To demonstrate the validity of the proposed method, numerical examples and machining are given in this section. The proposed algorithm is implemented in C++ with the 3D geometric modeler ACIS. Figure 6 presents the tested blade surface and the associated impeller model. The fillet radius on the blade root is 1 mm. A tapered ball-end cutter with the parameter $r_{\text{ball}} = 1$ mm, $\varphi = 5^{\circ}$, $H = 20$ mm is used in this case study. The five-axis machine tool utilized for the experimental tests is DMG Ultrasonic 10, which is a AC-type table-tilting machine tool, and the CNC system is SIEMENS 840D solutionline. The forward kinematics of this machine tool is expressed as

$$i = \sin(C) \times \sin(A), j = \cos(C) \times \sin(A), k = \cos(A).$$

Fifty cutter locations are first determined using the Chiou's method [29] combined with the bisection method to satisfy the hub surface gouge-free constraint [30]. The tolerance between the ball-end of the cutter and the hub surface is set 0.01 mm. After acquiring the cutter locations, the corresponding positions of the rotary axes for each cutter location can be calculated with the IKT of the machine tool [20]. The cutter reference point trajectory and the displacement curves of the two rotary axes along the initial path can be acquired by the interpolation method in Ref. [31], and the degree of B-spline curve here is 5. The evolutions of the two rotary axes A

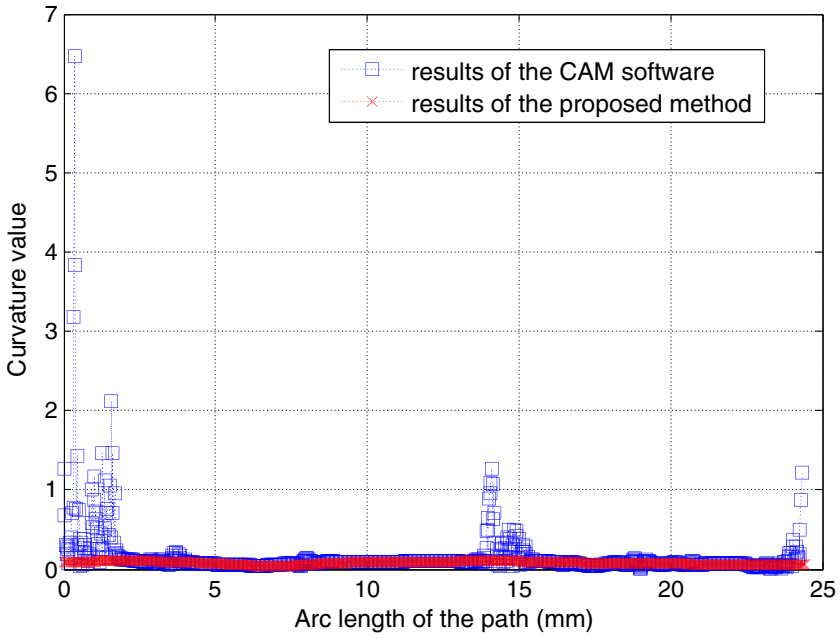

Fig. 11 Comparisons of the curvature value along $\boldsymbol{P}(u)$

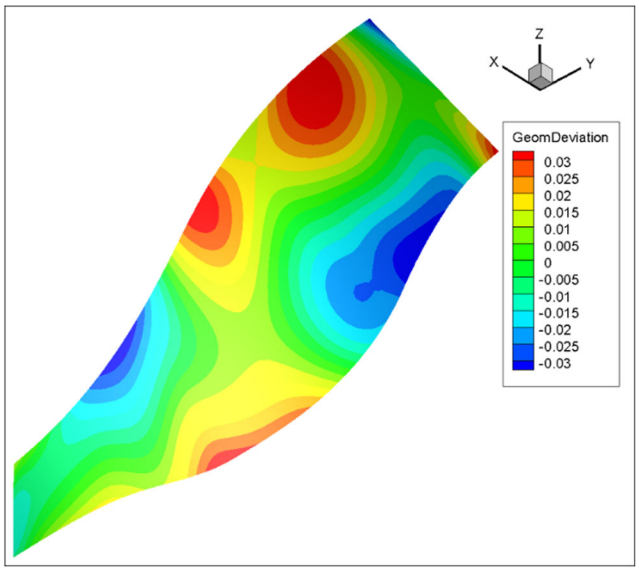

Fig. 12 Distribution of the geometric deviations

and C during the initial tool path are shown in Fig. 7. Curvature is chosen as an important criterion for motion curve because sharp bends in it mean strong motion changes. Thus, a cutter reference point trajectory with small curvature is preferred. The curvature plot for the cutter reference point trajectory of the initial path is given in Fig. 8, and oscillations can be found. For the initial path, the smoothness indicators in Eq. (10) are $F_{\text{first, }A}=0.049$, $F_{\text{second, }A}=1.8e-3$, $F_{\text{third, }A}=1.3e-3$, $F_{\text{first, }C}=0.063$, $F_{\text{second, }C}=4.5e-3$, $F_{\text{third, }C}=4.2e-3$, $F_{\text{first, }pt}=24.42$, $F_{\text{second, }pt}=0.461$, and $F_{\text{third, }pt}=7.145$.

To evaluate the geometric deviations, 100×30 points are sampled on the design surface, and 100 points are sampled on $\boldsymbol{P}(u)$. The parameters used in the algorithm to calculate the geometric deviations are $M=50$, $T=100$, and $CR=0.3$. The maximal undercut and overcut of the initial tool path are 0.0031 and 0.081 mm, respectively. The maximal undercut and gouging between the cutter's ball-end and the hub surface along the initial path are 0.0096 and 0.0098 mm, respectively, satisfying the specified tolerance.

Before using the SQP method to solve the smoothness flank milling path generation model, **P3** is solved to obtain a good initial solution first. $\lambda_{\text{penalty}}=1000$, and $n1$ and $n2$ in **P1** are 100×30 and 100, respectively. After three iterations, the maximal undercut and overcut of the obtained path are 0.018 and 0.012 mm, respectively. The maximal undercut and gouging between the cutter's ball-end and the hub surface are 0.003 and 0.0014 mm, respectively, which are controlled within the specified tolerance. In addition, the smoothness indicators in Eq. (10) become $F_{\text{first, }A}=0.046$, $F_{\text{second, }A}=1.2e-3$, $F_{\text{third, }A}=2.32e-5$, $F_{\text{first, }C}=0.043$, $F_{\text{second, }C}=1.1e-3$, $F_{\text{third, }C}=4.31e-5$, $F_{\text{first, }pt}=24.38$, $F_{\text{second, }pt}=0.174$, and $F_{\text{third, }pt}=0.0134$. The distributions of the geometric deviations of the paths before and after optimization are shown in Fig. 9.

A compromise between the geometric deviations and smoothness of the tool path has to be made to find a best tool path to ensure high-performance machining [7]. Therefore, the specified geometric tolerance is set 0.035 mm in this case. After the smoothness optimization with the SQP method setting the maximal number of iterations to 3, the smoothness indicators become $F_{\text{first, }A}=0.044$, $F_{\text{second, }A}=8.6e-4$, $F_{\text{third, }A}=1.84e-5$, $F_{\text{first, }C}=0.041$, $F_{\text{second, }C}=9.\ 8e-4$, $F_{\text{third, }C}=1.78e-5$, $F_{\text{first, }pt}=24.30$, $F_{\text{second, }pt}=0.159$, and $F_{\text{third, }pt}=8.6e-3$, which are all smaller than those of the initial solution. The evolutions of the two rotary axes along the optimized tool path are illustrated in Fig. 10, compared with those of the initial path. The curvature value along $\boldsymbol{P}(u)$ of the optimized path is also presented in Fig. 11. After the optimization, the positions of C axis along the path change more slowly, and the curvature values

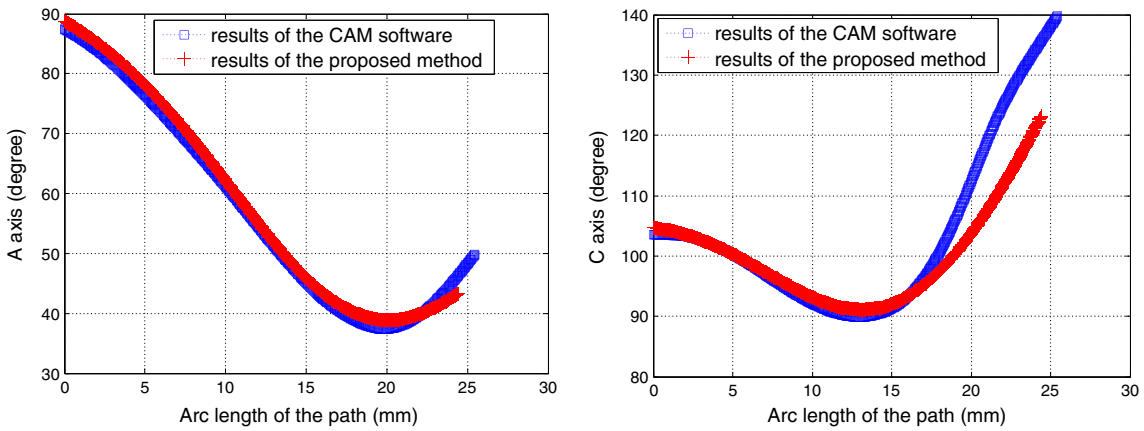

(a) Evolutions of A axis (b) Evolutions of C axis

Fig. 13 Comparisons of the evolutions of the two rotary axes

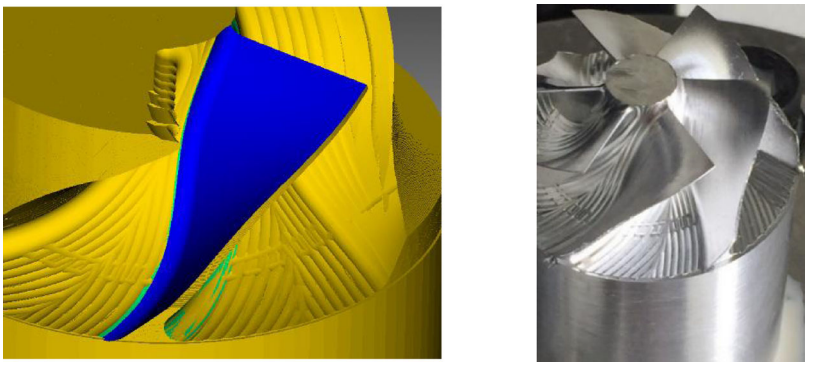

Fig. 14 The simulation and machining results

(a) Simulation result in Vericut

(b) The machined blade surface

along $\boldsymbol{P}(u)$ vary gently, indicating the effectiveness of the proposed method. Besides, the distribution of the geometric deviations of the optimized path is presented in Fig. 12, satisfying the specified geometric accuracy requirement.

*Remark: The computational time of the smoothness optimization with the SQP method depends on parameters n*1 and *n*2. *It is better to reduce the number of sampling points to shorten the computational time*.

The CAM Software MAX-PAC is employed to generate the blade surface flank milling path as well, and the results are used to compare with those of our method. The associated rotary axis displacements along the path are given in Fig. 13, as well as the results obtained with our method. It can conclude that the C axis movements of the path generated by our method are smoother than those obtained by the MAX-PAC. The curvature value along $\boldsymbol{P}(u)$ is also shown in Fig. 11, compared with that of our method. The curvature values at the beginning and end of the path generated with the CAM software, which are the engage and retract movements, are large. However, dramatic changes can be found in the curvature plot of the path, denoting the cutter reference point trajectory is not fairness.

Finish milling of the blade surface is also conducted. The material of the impeller is aluminum alloy 6061. Semi-finish is utilized to leave a uniform thickness allowance for finish milling. The finish cutting conditions are spindle speed = 8000 rpm, feed rate = 800 mm/min, and finish milling allowance = 0.3 mm. Both the paths generated by our method and the CAM software are used in the finish milling. The machined surfaces with these two methods are similar, and no tool marks are left on the machined surfaces. Figure 14a presents the simulation result milled by the path calculated with our method in the Vericut software, and Fig. 14b shows the photograph of the machined surface milled by the identical path. Even though the programmed feed rate in the finish milling is fixed, the planned tool path can also influence the machining time significantly. As can be seen from the CNC system, both the feed rates during the machining with the two paths change frequency. The CNC system can time the machining time, and the machining time of the path obtained with our method and the CAM software are 60 and 75 s respectively. The reason why our method's machining time is shorter is that the trajectory of the cutter reference point and the C axis movement generated by our method are smoother than those of the CAM software, and then the average feed rate during the machining is higher. The effectiveness of the developed method is thus experimentally confirmed.

5 Conclusions

This paper presents an approach to generate smooth five-axis flank milling tool paths for blade surfaces considering the geometric constraints of hub surface gouging-avoidance and accuracy. The algorithm smooths the rotary axis motions directly, and the cutter reference point trajectory is optimized as well. The sum of the squares of the first, second, and third derivatives of the displacement curves for the two rotary axes and the cutter reference point trajectory is adopted as the smoothness indicators. The smoothness optimization model is established as a constrained nonlinear optimization problem, and then the SQP and the Gauss-Newton methods are employed to solve the problems. Simulations and machining experiments have been carried out to confirm the practicability and effectiveness of the proposed method.

Funding information This work was supported by the Science and Technology Planning Project of Guangdong Province (Grant Numbers 2017B090913006 and 2016A010102019), the Science and Technology Planning Project of Guangzhou City (Grant Numbers 201504291036487 and 201604020124), and the China Postdoctoral Science Foundation (Grant Number 2018M633009).

Geometric deviation calculation based on DE algorithm

Input: The parameters of the DE algorithm: the maximal number of iterations (T), the size of population (M), the crossover probability (CR); the geometric parameters of the cutter; point $\boldsymbol{p}_l$ on the design surface;

Output: The parametric coordinate (a,u) of point $\boldsymbol{p}_l$ on the tool path satisfying Eq. (8) and the associated geometric deviation.

Step 0 (Initialization):

(1) Set $k=0$;

(2) Generate a $M\times 2$ matrix $\boldsymbol{A}$, each row of which represents an initial solution (a,u). Any component $A_{i,j}\,(i=0,1,\ldots,M-1;\ j=0,1)$ of $\boldsymbol{A}$ is determined as

$$\begin{aligned} A_{i,0} &= rand(0,1)\cdot(a_1-a_0)+a_0 \\ A_{i,1} &= rand(0,1)\cdot(u_l-u_p)+u_p \end{aligned} \tag{15}$$

where $rand(0,1)$ is a uniformly distributed random number lying between 0 and 1.

(3) Denote $f_i(a,u)=\left\|\boldsymbol{p}_l-\boldsymbol{S}(a,u)\right\|-r(a,u)$. Among the rows of $\boldsymbol{A}$, find out the best solution $f(a^*,u^*)$ such that $f(a^*,u^*)=\min\limits_{i\in\{0,1,\ldots,M-1\}} f_i(a,u)$. Let $\boldsymbol{A}_{best}=(a^*,u^*)$.

Step 1 (Iteration)

while $k\le T$ do

for all $i\le M-1$

Randomly select $p_1,p_2,p_3,p_4,p_5\in\{0,1,\ldots,M-1\}$ and $i\ne p_1\ne p_2\ne p_3\ne p_4\ne p_5$.

for all $j\le 1$

$$h_{i,j}=\begin{cases} A_{p_1,j}+F\cdot\left(A_{p_2,j}-A_{p_3,j}\right), & \text{if } k_{rand}=1 \\ A_{i,j}+F\cdot\left(A_{best,j}-A_{i,j}\right)+F\cdot\left(A_{p_1,j}-A_{p_2,j}\right), & \text{if } k_{rand}=2 \\ A_{best,j}+F\cdot\left(A_{p_1,j}-A_{p_2,j}\right), & \text{if } k_{rand}=3 \\ A_{best,j}+F\cdot\left(A_{p_3,j}-A_{p_4,j}\right)+F\cdot\left(A_{p_1,j}-A_{p_2,j}\right), & \text{if } k_{rand}=4 \\ A_{p_5,j}+F\cdot\left(A_{p_3,j}-A_{p_4,j}\right)+F\cdot\left(A_{p_1,j}-A_{p_2,j}\right), & \text{if } k_{rand}=5 \end{cases}$$

where $k_{rand}\in[1,2,3,4,5]$ is a randomly chosen index and F is generated in $[-1,1]$ from the uniform distribution. A random number $r_m\in(0,1)$ is generated and $F=\begin{cases} rand(-1,0), & \text{if } r_m>0.5 \\ rand(0,1), & \text{if } r_m<0.5 \end{cases}$.

end for all *j*

Calculate $\upsilon_j=\begin{cases} h_{i,j}, & \text{if } rand(0,1)<CR \text{ or } j=j_{rand} \\ A_{i,j}, & \text{else} \end{cases}$, where $j_{rand}\in[0,1]$ is a randomly chosen index.

if $a_0>\upsilon_0$, then $\upsilon_0=a_0$; if $a_1<\upsilon_0$, then $\upsilon_0=a_1$; if $u_p>\upsilon_1$, then $\upsilon_1=u_p$; if $u_l<\upsilon_1$, then $\upsilon_1=u_l$.

Calculated $f_i(\upsilon_0,\upsilon_1)$, and then save the individuals A_i and $\boldsymbol{\upsilon}$ in a new population *P*.

end for all *i*

Sort the individuals in the population *P* according to their fitness, and then select the top *M* individuals to be the individuals in the next generation. The best individual can also be determined.

Clear the individuals in population *P*, and *k* = *k*+*1*.

end while

The Gauss-Newton method of solving P3

Equation (14) can be written as

$$\min_{\mathrm{w}\in\mathbb{R}^{\mathrm{m}}} F = \lambda_{\mathrm{ls}}\cdot\sum_{\mathrm{i}=0}^{\mathrm{n1}}\left[d_{\mathbf{p}_i,\boldsymbol{X}}(\boldsymbol{w})\right]^2 + \boldsymbol{w}^{\mathrm{T}}\boldsymbol{Y}\boldsymbol{w} + \lambda_{\mathrm{penalty}}\cdot\sum_{\mathrm{i}=0}^{\mathrm{n2}}\left(d_{\boldsymbol{c}_i,\boldsymbol{S}_0}(\boldsymbol{w})-r_{\mathrm{ball}}\right)^2 \tag{16}$$

Let $\boldsymbol{w}^{\mathrm{k}}$ be a candidate solution to Eq. (16) in the kth iteration and consider a perturbation of the form $\boldsymbol{w}^{\mathrm{k}}+\Delta\boldsymbol{w}^{\mathrm{k}}$. The object function becomes

$$\min_{\Delta\mathrm{w}\in\mathbb{R}^{\mathrm{m}}} F = \lambda_{\mathrm{ls}}\cdot\sum_{\mathrm{i}=0}^{\mathrm{n1}}\left[d_{\mathbf{p}_i,\boldsymbol{X}}(\boldsymbol{w}^{\mathrm{k}})+\Delta d_{\mathbf{p}_i,\boldsymbol{X}}(\boldsymbol{w}^{\mathrm{k}})\right]^2 + \lambda_{\mathrm{penalty}}\cdot\sum_{\mathrm{i}=0}^{\mathrm{n2}}\left[d_{\boldsymbol{c}_i,\boldsymbol{S}_0}(\boldsymbol{w}^{\mathrm{k}})+\Delta d_{\boldsymbol{c}_i,\boldsymbol{S}_0}(\boldsymbol{w}^{\mathrm{k}})\right]^2 + \left[(\boldsymbol{w}^{\mathrm{k}})^{\mathrm{T}}\boldsymbol{Y}^{\mathrm{k}}(\boldsymbol{w}^{\mathrm{k}})+2(\boldsymbol{w}^{\mathrm{k}})^{\mathrm{T}}\boldsymbol{Y}^{\mathrm{k}}(\Delta\boldsymbol{w}^{\mathrm{k}})+(\Delta\boldsymbol{w}^{\mathrm{k}})^{\mathrm{T}}\boldsymbol{Y}^{\mathrm{k}}(\Delta\boldsymbol{w}^{\mathrm{k}})\right] \tag{17}$$

Compute the displacement vector $\Delta\boldsymbol{w}^{\mathrm{k}}$ for the control points $\boldsymbol{w}^{\mathrm{k}}$ by minimizing Eq. (17). Therefore, $\Delta\boldsymbol{w}^{\mathrm{k}}$ can be found by calculating

$$\Delta\boldsymbol{w}^{\mathrm{k}} = \left[\lambda_{\mathrm{ls}}\cdot(\mathbf{A}_1{}^{\mathrm{k}})^{\mathrm{T}}(\mathbf{A}_1{}^{\mathrm{k}})+\lambda_{\mathrm{penalty}}\cdot(\mathbf{A}_2{}^{\mathrm{k}})^{\mathrm{T}}(\mathbf{A}_2{}^{\mathrm{k}})+\boldsymbol{Y}^{\mathrm{k}}\right]^{-1}\cdot\left(\lambda_{\mathrm{ls}}\cdot(\mathbf{A}_1{}^{\mathrm{k}})^{\mathrm{T}}\mathbf{b}_1{}^{\mathrm{k}}+\lambda_{\mathrm{penalty}}\cdot(\mathbf{A}_2{}^{\mathrm{k}})^{\mathrm{T}}\mathbf{b}_2{}^{\mathrm{k}}-(\boldsymbol{w}^{\mathrm{k}})^{\mathrm{T}}\boldsymbol{Y}^{\mathrm{k}}\right) \tag{18}$$

where $\boldsymbol{A}_1=\begin{bmatrix}\nabla d_{\mathbf{p}_0,\boldsymbol{X}}(\boldsymbol{w}^{\mathrm{k}})^{\mathrm{T}}\\ \vdots\\ \nabla d_{\mathbf{p}_{n_1},\boldsymbol{X}}(\boldsymbol{w}^{\mathrm{k}})^{\mathrm{T}}\end{bmatrix}$, $\boldsymbol{A}_2=\begin{bmatrix}\nabla d_{\boldsymbol{c}_0,\boldsymbol{S}_0}(\boldsymbol{w}^{\mathrm{k}})^{\mathrm{T}}\\ \vdots\\ \nabla d_{\boldsymbol{c}_{n2},\boldsymbol{S}_0}(\boldsymbol{w}^{\mathrm{k}})^{\mathrm{T}}\end{bmatrix}$, $\boldsymbol{b}_1=\begin{bmatrix}d_{\mathbf{p}_0,\boldsymbol{X}}(\boldsymbol{w}^{\mathrm{k}})\\ \vdots\\ d_{\mathbf{p}_{n1},\boldsymbol{X}}(\boldsymbol{w}^{\mathrm{k}})\end{bmatrix}$, and $\boldsymbol{b}_2=\begin{bmatrix}d_{\boldsymbol{c}_0,\boldsymbol{S}_0}(\boldsymbol{w}^{\mathrm{k}})\\ \vdots\\ d_{\boldsymbol{c}_{n2},\boldsymbol{S}_0}(\boldsymbol{w}^{\mathrm{k}})\end{bmatrix}$. Please note that the weightings λ_{ls}, λ_{A}, and λ_{C} are change in each iteration. Replacing the control points by $\boldsymbol{w}^{\mathrm{k}+1}=\boldsymbol{w}^{\mathrm{k}}+\Delta\boldsymbol{w}^{\mathrm{k}}$ and repeating these steps until convergence, that is, until the maximal number of iterations is reached or the incremental change of the control points falls below a prescribed threshold.

References

1. Fan HZ, Wang SJ, Xi G, Cao YL (2017) A novel tool-path generation method for five-axis flank machining of centrifugal impeller with arbitrary surface blades. Proc Inst Mech Eng B J Eng Manuf 231(1):155–166
2. Calleja A, Alonso M, Fernández A, Tabernero I, Ayesta I, Lamikiz A, López de Lacalle L (2015) Flank milling model for tool path programming of turbine blisks and compressors. Int J Prod Res 53(11):3354–3369
3. Calleja A, Bo PB, González H, Bartoň M, López de Lacalle LN (2018) Highly accurate 5-axis flank CNC machining with conical tools. Int J Adv Manuf Technol 97:1605–1615
4. Lu YA, Bi QZ, Zhu LM (2016) Five-axis flank milling of impellers: optimal geometry of a conical tool considering stiffness and geometric constraints. Proc Inst Mech Eng B J Eng Manuf 230(1):38–52
5. Huang ND, Bi QZ, Wang YH, Sun C (2014) 5-Axis adaptive flank milling of flexible thin-walled parts based on the on-machine measurement. Int J Mach Tool Manu 84:1–8
6. Tournier C, Castagnetti C, Lavernhe S, Avellan F (2006) Tool path generation and post-processor issues in five-axis high speed machining of hydro turbine blades. Fifth International Conference on High Speed Machining, Metz, France
7. Pechard PY, Tournier C, Lartigue C, Lugarini JP (2009) Geometrical deviations versus smoothness in 5-axis high-speed flank milling. Int J Mach Tool Manu 49(6):454–461
8. Wang N, Tang K (2007) Automatic generation of gouge-free and angular-velocity-compliant five-axis toolpath. Comput Aided Des 39(10):841–852
9. Kim YJ, Elber G, Bartoň M, Pottmann H (2015) Precise gouging-free tool orientations for 5-axis CNC machining. Comput Aided Des 58:220–229
10. Zheng G, Bi QZ, Zhu LM (2012) Smooth tool path generation for five-axis flank milling using multi-objective programming. Proc Inst Mech Eng B J Eng Manuf 226(2):247–254
11. Affouard A, Duc E, Lartigue C, Langeron JM, Bourdet P (2004) Avoiding 5-axis singularities using tool path deformation. Int J Mach Tool Manu 44(4):415–425
12. Castagnetti C, Duc E, Ray P (2008) The domain of admissible orientation concept: a new method for five-axis tool path optimisation. Comput Aided Des 40(9):938–950
13. Beudaert X, Pechard PY, Tournier C (2011) 5-Axis tool path smoothing based on drive constraints. Int J Mach Tool Manu 51(12):958–965
14. Plakhotnik D, Lauwers B (2014) Graph-based optimization of five-axis machine tool movements by varying tool orientation. Int J Adv Manuf Technol 74(1–4):307–318

15. Lin ZW, Fu JZ, Shen HY, Gan WF (2014) Non-singular tool path planning by translating tool orientations in C-space. Int J Adv Manuf Technol 71(9–12):1835–1848
16. Lin ZW, Fu JZ, Yao XH, Sun YF (2015) Improving machined surface textures in avoiding five-axis singularities considering tool orientation angle changes. Int J Mach Tool Manu 98:41–49
17. Geng L, Zhang YF (2015) Generation of kinematic smooth toolpaths in 5-axis milling of sculptured surfaces. Int J Manuf Res 10(3):237–266
18. Hu PC, Tang K (2016) Five-axis tool path generation based on machine-dependent potential field. Int J Comput Integr Manuf 29(6):636–651
19. Srijuntongsiri G, Makhanov SS (2015) Optimisation of five-axis machining G-codes in the angular space. Int J Prod Res 53(11): 3207–3227
20. Lu YA, Ding Y, Zhu LM (2016) Smooth tool path optimization for flank milling based on the gradient-based differential evolution method. J Manuf Sci Eng 138(8):081009
21. Lu YA, Bi QZ, Zhu LM (2016) Five-axis flank milling tool path generation with smooth rotary motions. Procedia CIRP 56:161–166
22. Mi ZP, Yuan CM, Ma XH, Shen LY (2017) Tool orientation optimization for 5-axis machining with C-space method. Int J Adv Manuf Technol 88(5–8):1243–1255
23. Lartigue C, Duc E, Affouard A (2003) Tool path deformation in 5-axis flank milling using envelope surface. Comput Aided Des 35(4):375–382
24. Piegl L, Tiller W (1997) The NURBS book. Springer Verlag, Berlin
25. Zhu LM, Zheng G, Ding H, Xiong YL (2010) Global optimization of tool path for five-axis flank milling with a conical cutter. Comput Aided Des 42(10):903–910
26. Zhu LM, Zhang XM, Zheng G, Ding H (2009) Analytical expression of the swept surface of a rotary cutter using the envelope theory of sphere congruence. J Manuf Sci Eng 131(4):041017
27. Das S, Suganthan P (2011) Differential evolution: a survey of the state-of-the-art. IEEE Trans Evol Comput 15(1):4–31
28. Trivedi A, Sanyal K, Verma P, Srinivasan D (2017) A unified differential evolution algorithm for constrained optimization problems. IEEE Congress on Evolutionary Computation (CEC) 2017: 1231–1238
29. Chiou JCJ (2004) Accurate tool position for five-axis ruled surface machining by swept envelope approach. Comput Aided Des 36(10):967–974
30. Tang M, Zhang DH, Luo M, Wu BH (2012) Tool path generation for clean-up machining of impeller by point-searching based method. Chin J Aeronaut 25(1):131–136
31. Langeron JM, Duc E, Lartigue C, Bourdet P (2004) A new format for 5-axis tool path computation, using Bspline curves. Comput Aided Des 36(12):1219–1229